Hindawi Publishing Corporation
Mathematical Problems in Engineering
Volume 2014, Article ID 573962, 13 pages
http://dx.doi.org/10.1155/2014/573962

Research Article

Dynamic and Static Combination Analysis Method of Slope Stability Analysis during Earthquake

Liang Lu,[1,2] Zongjian Wang,[3] Xiaoyuan Huang,[1,2] Bin Zheng,[1,2] and Katsuhiko Arai[4]

[1] *School of Civil Engineering, Chongqing University, Chongqing 400045, China*
[2] *Key Laboratory of New Technology for Construction of Cities in Mountain Area, Chongqing University, Ministry of Education, Chongqing 400045, China*
[3] *Institute of Geotechnical Engineering, Chongqing Jiaotong University, Chongqing 400074, China*
[4] *Institute of Ground Disaster Prevention in Fukui, Fukui 910-0004, Japan*

Correspondence should be addressed to Liang Lu; luliangsky@163.com

Received 12 June 2014; Accepted 28 August 2014; Published 12 October 2014

Academic Editor: Gen Qi Xu

The results of laboratory model tests for simulating the slope failure due to vibration, including unreinforced slope and the slope reinforced by using geotextile, show that the slope failure occurs when a cumulative plastic displacement exceeds a certain critical value. To overcome the defects of conventional stability analysis, which evaluates the slope characteristics only by its strength parameters, a numerical procedure considering the stiffness and deformation of materials and geosynthetics is proposed to evaluate the seismic slope stability. In the proposed procedure, the failure of slope is defined when the cumulative plastic displacement calculated by a dynamic response analysis using actual seismic wave exceeds the critical value of displacement estimated by a static stability analysis considering seismic coefficient. The proposed procedure is applied to the laboratory model tests and an actual failure of slope in earthquake. The case study shows the possibility that the proposed procedure gives the realistic evaluation of seismic slope stability.

1. Introduction

Engineering practitioners and researchers have shown a growing interest in analytical procedures for assessing the seismic stability of slopes. Failure of slope by earthquake usually has some characteristics including wide distribution, large numbers, and high-speed velocity. Researches have shown that landslides or failure of slope triggered by recent seismic events can result in significant human and financial losses and severe environmental impact [1–3]. Thus, it shows that studies on dynamic stability of slope have important engineering and social significance.

In spite of many research studies that analyzed slope stability, it is difficult to realistically evaluate the slope stability during earthquake. Whether a particular slope produces a collapse in an earthquake depends on details of material strength, slope configuration, ground motion, and so forth [4]. The conventional stability analysis based on the limit equilibrium method has been often employed in practical design works by considering static inertia force due to seismic intensity [5, 6]. Stability analyses of earth slopes during earthquake shaking were initiated using what has come to be known as the pseudostatic method [7]. The horizontal inertial force is expressed as the product of a seismic coefficient and the weight of the potential sliding mass [8]. Since this method evaluates the slope characteristics only by its strength parameters, it cannot easily relate the seismic intensity to the actual time history [9]. And it is also difficult to consider spatial distribution of seismic acceleration, deformation characteristics of slope, the stiffness and materials playing an important role for evaluating earth reinforcement method, and so forth; the conventional stability analysis often tends to become uncertain and unreliable for a slope consisting of multiple layers or including materials having quite different stiffness, for instance, reinforced slope with geotextile. A slope stability analysis based on a rigid plastic dynamic model

Table 1: Specification of shaking table.

Excitation direction	Size	Loading capacity	Excited force	Maximum amplitude of displacement	Load mode	Frequency
Horizontal · vertical	1.5 m × 1.5 m	19.6 kN	Static pressure bearing	Horizontal: ±80 kN, vertical: ±40 kN	Horizontal: ±75 mm, vertical: ±50 mm	0.1~50 Hz

is proposed, but it appears to require a lot of numerical efforts and to contain a certain numerical difficulty in some cases [10]. Due to these defects, some analytical methods of dynamic deformation are proposed based on equivalent linear analysis, stress-deformation analysis, and Newmark method, and so forth [11–13]. When using the dynamic stress-deformation analysis which tries to simulate seismic behavior of slope, most of the classic FE analysis are not easy to define an explicit collapse state.

In this paper, we carry out a series of shaking table tests for vertical filling slope with and without earth reinforcement by varying acceleration amplitude and frequency. According to the test results, a slope failure during earthquake occurs when a cumulative plastic deformation of slope exceeds a certain critical value and the deformation just before slope failure is constant value independently of acceleration amplitude and frequency; we propose a numerical procedure to evaluate the slope stability during earthquake, in which the cumulative plastic deformation is calculated by a dynamic stress-deformation analysis using an actual seismic wave, and the critical value of deformation is estimated by a static stability analysis considering seismic intensity. The proposed procedure is applied to the laboratory model test and one case of actual slope failure; the effects of seismic wave and earth reinforcement are investigated. The results show that the proposed method is a feasible, accurate, and effective method for estimating the stability of slope during earthquake.

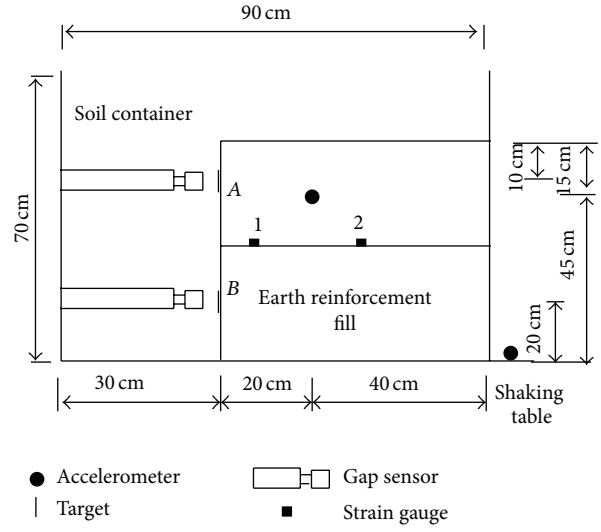

Figure 1: Experimental setup.

Table 2: The parameters of fills.

Grain gradation			Density	Optimum water content	Maximum dry density
Gravel	Sand	Silt			
9.64%	88.78%	1.58%	2.40 g/cm^3	15.5%	1.74 g/cm^3

2. Laboratory Model Test

The model tests of vertical fill slope on shaking table are carried out to research the relationship of failure deformation of slope due to vibration and acceleration amplitude or frequency. The reason of modeling the slope as a vertical fill is that the ordinary inclined slope cannot collapse easily due to insufficient height of model slope, and it is not easy for sloped fill to be sufficiently consolidated. In the model tests the influence of earth reinforcement is also discussed.

2.1. Experimental Facilities. The laboratory model tests for vertical fill made of mountain sand 60 cm wide, 30 cm thick, and 60 cm high are carried out in a steel soil tank. Figure 1 shows the view of soil tank and the experimental setup of vertical fill model test system. Two accelerometers and two gap sensors are provided in the corresponding position in Figure 1. For the fill reinforced by earth reinforcement, one layer of geotextile 30 cm in width and 60 cm in length is placed in the 30 cm depth of vertical fill. Two strain gauges are attached to the geotextile as shown in Figure 1 to measure the tensile stress of geotextile during the deformation of fill. The specification of shaking table is shown in Table 1. The parameters of soil used in the model vertical fill are given as Table 2.

2.2. Test Procedure and Measurements. Plane strain conditions are considered for all model tests. In order to reduce the friction between fill and sidewall of soil container, a thin rubber membrane smeared with silicon grease is pasted on both sidewalls of soil tank. A layer of nonwoven textile is paved in the bottom of soil tank, so as to constrain the horizontal deformation along the bottom surface. To leave enough space before the vertical fill shown in Figure 1, a steel brace is used to support the vertical fill. The model of fill slope is made in three steps. First, put the mountain sand in the optimum water content into the height of 32 cm and apply the pressure of 29.4 kN/m^2 by air cylinder to a bearing plate with the same size as the horizontal plane of soil tank for 10 minutes. Subsequently the mountain sand is put to height of 47 cm, and then the accelerometers are set after the sand stratum is consolidated through the bearing plate and

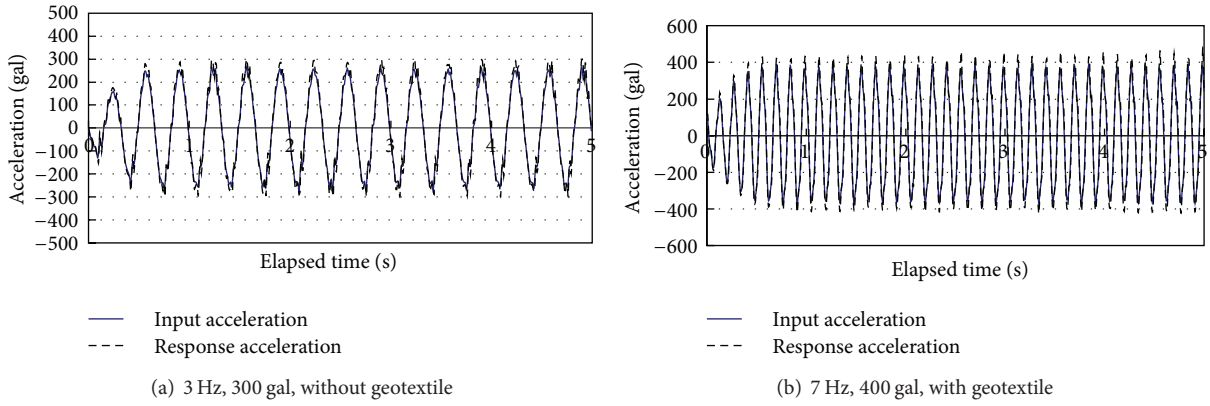

(a) 3 Hz, 300 gal, without geotextile

(b) 7 Hz, 400 gal, with geotextile

Figure 2: Time history of response acceleration.

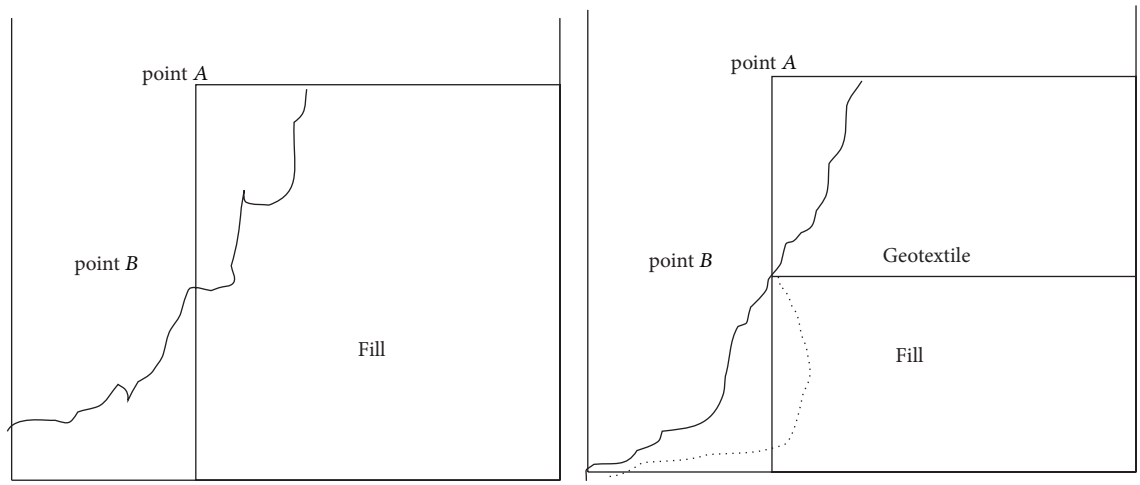

(a) Model slope without earth reinforcement

(b) Model slope with earth reinforcement

Figure 3: Failure patterns of vertical slope.

hammer with weight of 2.1 kN/m^2 for 5 minutes. Finally, the mountain sand is filled into the soil container of 64 cm in height. As the same procedure stated above, a bearing plate is used for consolidating the soil layer by air cylinder with a pressure of 29.4 kN/m^2 keeping 10 minutes.

Two targets are inserted into the vertical side of 20 cm in height and 50 cm of the fill, respectively, and two gap sensors are installed correspondingly as shown in Figure 1. If we use one-time filling of the mountain sand to predetermined position and compress it by air cylinder, it is difficult to obtain a stable vertical fill due to insufficient consolidation. A stable vertical fill is made by consolidating the mountain sand in two steps as stated above. For the case of reinforced subsoil, the construction of fill is the same as above in addition to one layer of earth reinforcement placed at the height of 32 cm in soil tank.

Combining two kinds of frequency of 3 Hz and 7 Hz and three types of acceleration amplitude of 200, 300, and 400 gal, six sinusoids are provided for the vertical fill on shaking table. For each case, the experiment is carried out five times due to the dispersion of experimental results.

From the vibration tests, the acceleration of the corresponding position, the horizontal deformation of vertical side of fill, and vibration time until the collapse of vertical slope were measured. The acceleration and the horizontal deformation were measured, respectively, by accelerometer with capacity of 1960 gal and gap sensor with ±7.5 mm of measuring range. And the elapsed time until collapse was measured by stopwatch at the moment when the filling was observed to begin to collapse. The same vibration tests are performed for the case with earth reinforcement, in which the tensile stress was also measured.

2.3. Test Results. Figure 2 exemplifies the time history of response acceleration using two cases with different frequency and amplitude of acceleration a_m. It demonstrates that the response acceleration spectrum at the location of testing shown in Figure 1 agrees approximately with the input acceleration. Figure 3 shows the failure modes for nonreinforced and reinforced vertical filling slope. Note that it is impossible to get the same position of slip surface in different sinusoids, but the collapse mode obtained from experimental

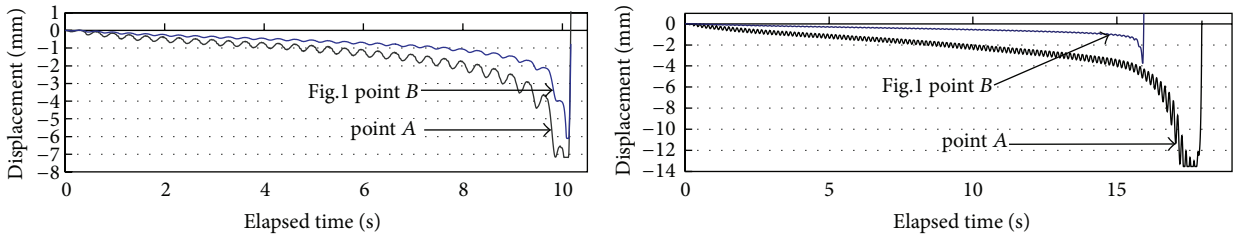

(a) 3 Hz, 300 gal, without geotextile

(b) 7 Hz, 300 gal, with geotextile

Figure 4: Time history of horizontal displacement.

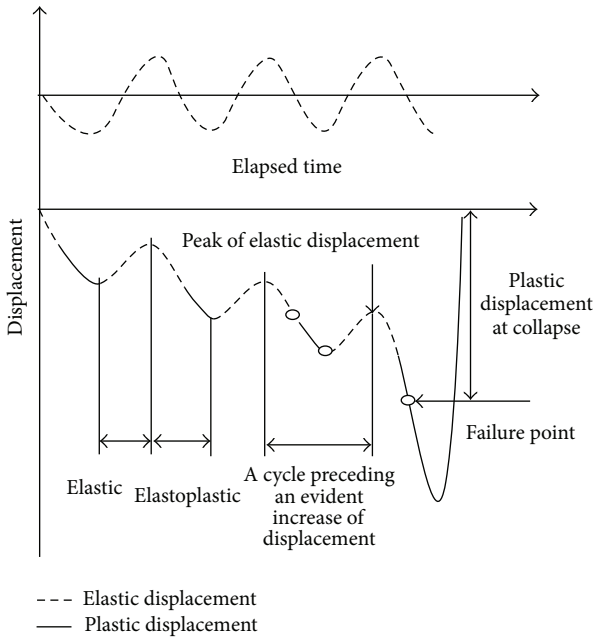

Figure 5: Definition of displacement at collapse.

results showed similar regular pattern. For the nonreinforced case, Figure 3(a) shows that the collapse occurs from the upper region corresponding to point A through the bottom region below point B of vertical filling at the same time. The collapse pattern of filling reinforced with geotextile shown in Figure 3(b) shows that a small-scale failure first occurred in the region around point B below the geotextile in the form of broken line, and the loosened upper subsequently collapsed. In this paper, the vertical filling slope is assumed to be collapsed when the small-scale collapse occurs in the reinforced subsoil.

In this paper, we must define "displacement at collapse" rigorously, because we try to express the collapse of fill based on the plastic displacement. To explain the definition of "displacement at collapse," the time history of horizontal displacement until the collapse at a certain frequency and amplitude of acceleration is shown in Figure 4, in which a remarkable increase in horizontal displacement at collapse occurs. As shown in Figure 5, the horizontal deformation is thought to be equal to the superposition of the elastic and the unrecoverable plastic displacements. The "plastic displacement at collapse" is defined to be occurred in the cycle with an evident and sudden increase in displacement. It is the sum of the plastic displacement at the cycle having sudden increase and the cumulative displacements of all preceding cycles.

For the vertical filling without earth reinforcement, because the upper and lower parts of vertical filling collapse at the same time, it is easy to define the plastic displacement at collapse as point A in Figure 1. Based on the aspect, the plastic displacements at collapse of point A for all cases are measured and shown in Figure 6(a). For each case, five groups of tests are carried out to ensure the reliability of test results. As shown in Figure 6, although the test results disperse, the plastic displacement at collapse remains in the range of 3.5 mm~7.5 mm and the average values are all close to 5.0 mm in any case. This shows that the plastic displacement at collapse is constant regardless of acceleration amplitude and frequency. For the reinforced fill, because the region below the earth reinforcement first collapsed, the horizontal deformation of point A located above the reinforced region directly is affected by the position of earth reinforcement, especially when failure of the filling below the earth reinforcement occurs. Thus in the case of reinforced slope, the plastic deformation at collapse is represented by point B in Figure 1. The measured plastic displacements at collapse of point B are shown in Figure 6(b). There is no measured plastic deformation at collapse for the seismic wave when $a_m = 200$ gal because the reinforced slope did not reach the state of collapse.

Figure 7 shows the elapsed time until collapse according to the above definition of collapse. It shows the elapsed time until collapse gets shorter as the acceleration amplitude increases, in the meantime the elapsed time for the frequency of 3 Hz is a little longer than 7 Hz in most cases. The measured elapsed time until collapse for reinforced filling slope extended as compared with that of the nonreinforced filling slope.

3. Numerical Procedure

Figures 4 and 5 suggest that the slope failure occurs when the cumulative plastic displacement exceeds a certain critical value. From this, a slope can be considered to be collapsed when the cumulative plastic displacement reaches a specified value of plastic displacement at collapse from Figure 6,

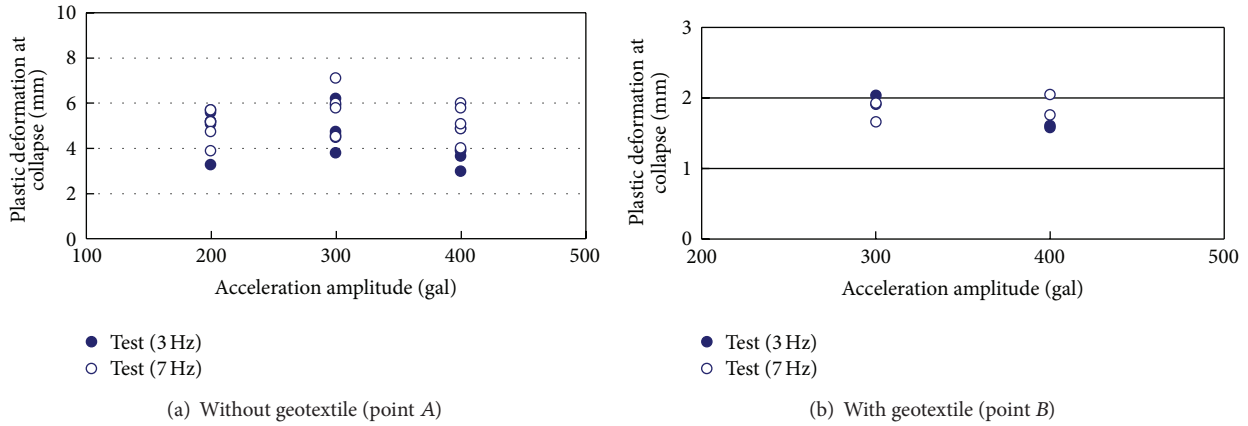

(a) Without geotextile (point A) (b) With geotextile (point B)

Figure 6: Plastic displacements at collapse in different seismic wave.

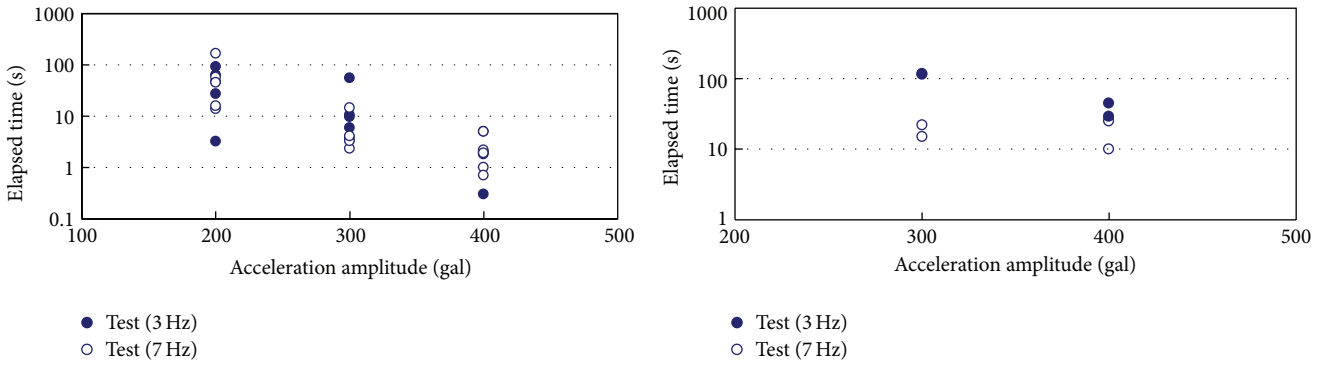

(a) Without geotextile (point A) (b) Without geotextile (point B)

Figure 7: Measured duration until the collapse of slope in different seismic wave.

which shows that the plastic displacement at collapse is independent of the acceleration amplitude and frequency. However, it is difficult to calculate the plastic displacement at collapse explicitly by a dynamic response analysis, because the displacement increases monotonously with elapsed time without a clear turning point in most cases. Based on the points above, we propose a new numerical procedure. In the proposed procedure the plastic displacement at collapse is estimated by a static stability analysis, because it may define the collapse state more easily. The cumulative plastic displacement is calculated by a dynamic response analysis. It is not certain whether the static stability analysis and dynamic response analysis provide the same result of plastic displacement at collapse, but it can be presumed from the test results given before that the plastic displacement at collapse is the same with the value of static stability analysis since it is in connection only with the characteristics of slope irrelative to the acceleration amplitude and frequency. In view of this assumption, the slope is considered to be collapsed when the cumulative plastic deformation calculated by dynamic response analysis exceeds the plastic deformation at collapse decided by static stability analysis. Based on the above results, we can calculate the elapsed time until collapse. Figure 8 shows FE meshing of the vertical filling slope used in the analysis, in which one layer of geotextile located in the middle for reinforced slope.

3.1. Static Stability Analysis. It is difficult to express the deformation in the conventional limit equilibrium method and to define the collapse for the FE analysis employing nonlinear stress-strain models. The static stability analysis aims at calculating the deformation at collapse. Employing Mohr-Coulomb yield criterion and an initial stress method, a numerical procedure in the static stability analysis is applied to define the collapse mode by the distribution of yield elements and to calculate the deformation at collapse. Mohr-Coulomb and Coulomb yield criteria are, respectively, employed to vertical filling and friction interface.

Mohr-Coulomb criterion is as follows:

$$F_M = \left\{\left(\sigma_x - \sigma_y\right)^2 + 4\tau_{xy}^2\right\}^{1/2} - \left\{\left(\sigma_x + \sigma_y\right)\sin\varphi + 2c\cos\varphi\right\} = 0. \quad (1)$$

Coulomb yield criterion is as follows:

$$F_C = \left|\tau_{\mathrm{st}}\right| - c - \sigma_t \tan\varphi, \quad (2)$$

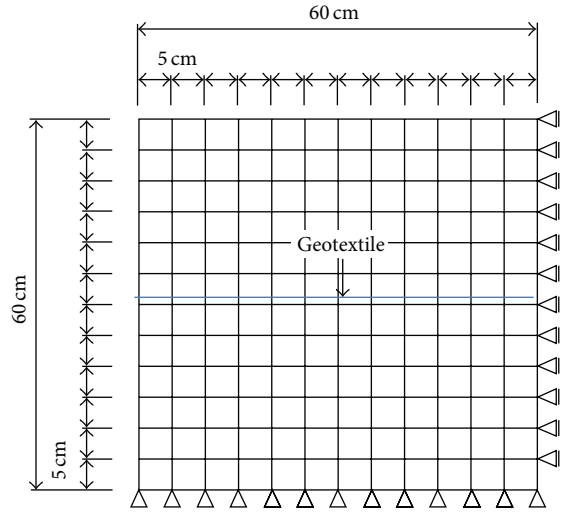

Figure 8: FE meshing in numerical analysis.

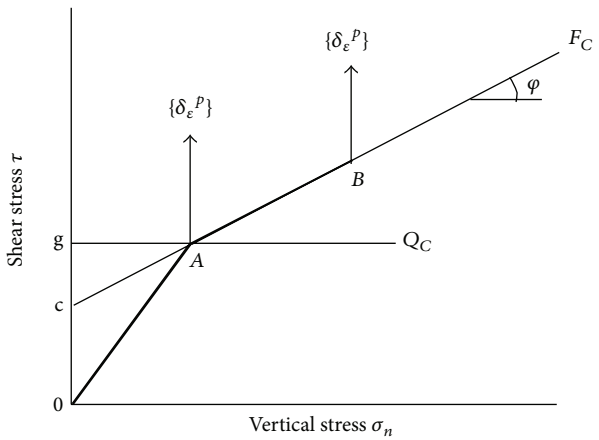

Figure 9: Flow rule followed by yield criterion curve.

where, σ_x, σ_y, and τ_{xy} are stress components and σ_t and τ_{st} are normal and shear stresses in friction interface.

In order to simulate the actual behavior, a perfect elastoplastic model is employed for constant σ_3 or normal stress of shear band σ_n. A linear elastic response is assumed before yielding state, while the perfectly plastic state corresponds to the limit state employing Cam-Clay model and Ouda model. For Coulomb interface, when applied further after yield point A, the stress state is assumed to move along yield surface from point A to B with a simple nonassociated flow rule, as shown in Figure 9, where F_C: yield function, Q_C: plastic potential, $Q_C = |\tau| - g = 0$; $\{\delta\varepsilon^p\}$: increment of plastic strain, and g: a hypothetical parameter which is not cited actually, because Q_C is used only by its differential form. In the limit equilibrium analysis, the stability analysis of slope is evaluated mainly by the final state of soil. The distribution of yield elements, calculated by the initial stress method presented by Zienkiewicz et al. [15, 16], is relatively in accordance with the final collapse pattern of slope. Figure 10 illustrates the initial stress method at only one loading stage.

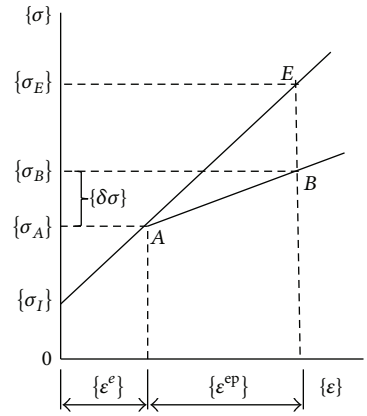

Figure 10: Initial stress method.

The fundamental flow diagram of calculation is shown in Figure 11, in which $\{u\}$: nodal displacement vector, $[K]$: stiffness matrix, $\{f\}$: total load vector, $[B]$: matrix for calculating strains from $\{u\}$, and V: volume of the element. Initial stress $\{\sigma_0\}$ is determined finally by employing the iteration loop shown in Figure 11. The numerical steps of the initial stress method are employed as follows. Step (1): assume the trial values of initial stress to be zero. Step (2): according to the following steps from (a) to (e), determine the initial stress $\{\sigma_0\}$ in each finite element. (a) Applying both total load vector $\{f\}$ and correction load vector $\{f_0^i\}$ due to $\{\sigma_0\}$, solve the following elastic problem

$$[K]\left\{u^i\right\} = \{f\} + \left\{f_0^i\right\}, \tag{3}$$

where i denotes a cycle of iteration for the initial stress method. (b) Find the yield elements. (c) For the yield elements, determine yield stress $\{\sigma_A\}$ by using the technique presented by Nayak and Zienkiewicz [17]. (d) Calculate $\{\sigma_B\}$ shown in Figure 10 by using $\{\sigma_A\}$ determined at step (c). (e) Modify initial stress $\{\sigma_0\}$ by

$$\{\sigma_{0i}\} = \{\sigma_{Ei}\} - \{\sigma_{Bi}\}. \tag{4}$$

Step (3): Replacing the initial stresses at the first cycle with those obtained at the preceding stage, the above iteration stage must be repeated until the results converge reasonably well. The initial stress method is the technique of an iterative procedure to search for the residual between outside force and equivalent load at joint as the load used in the next step. Combined with the assumptions of nonlinear stress-strain relationship and nontensile material for soil elements, the initial stress method provides approximate results. All elements of filling are assumed to bear no tensile stress, and reinforcement material is assumed to sustain no compression stress.

3.2. Dynamic Response Analysis. The objective of dynamic response analysis is to calculate the cumulative plastic displacement during vibration. The relationship of rigidity and damping constant versus strain is given in terms of the Hardin-Drnevich model shown in Figure 12, in which

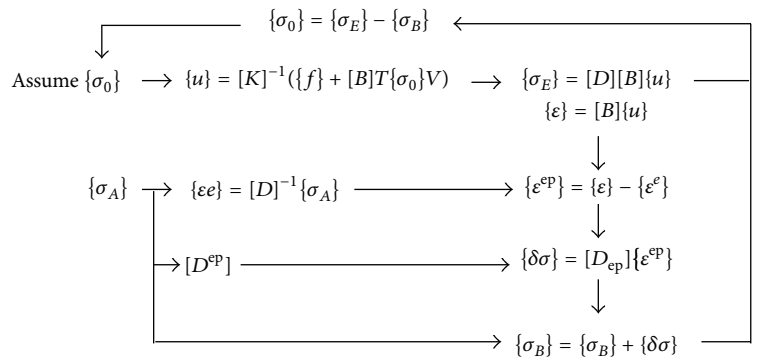

Figure 11: Flow diagram of calculation.

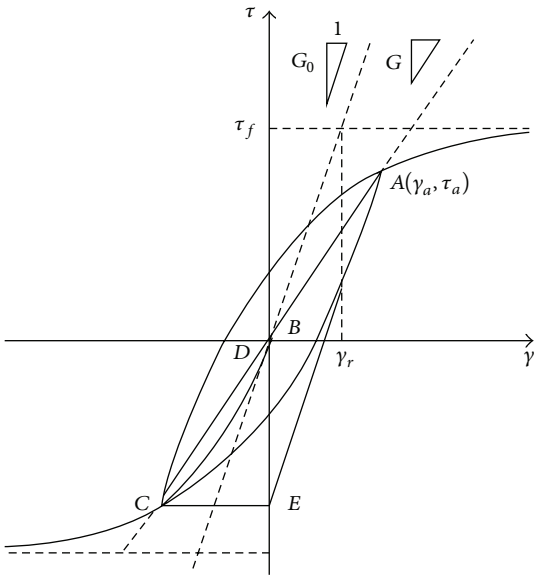

Figure 12: Hardin-Drnevich model.

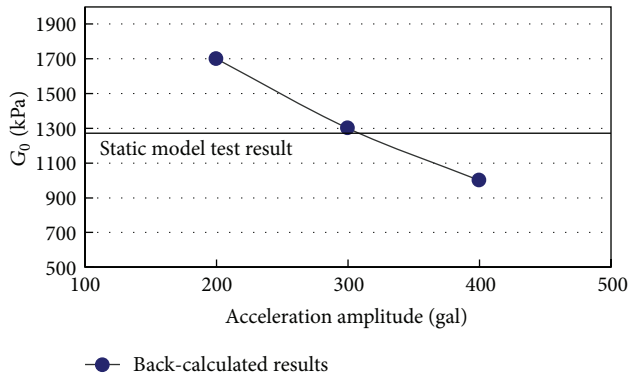

Figure 13: Back-calculated G_0 from model tests.

G: shear modulus, G_0: initial shear modulus, and $\gamma_r = \tau_f/G_0$. Employing the equivalent linearization technique, the analysis approximately simulates the variation of deformation modulus E and damping constant h. A direct integral is performed by Newmark-β method introduced by Smith [18]:

$$\begin{aligned}
&\left(\left(\alpha + \frac{1}{\vartheta}\Delta t\right)[M] + (\beta + \vartheta\Delta t)[K]\right) r_n \\
&= \vartheta\Delta t\{F_n\} + (1-\vartheta)\Delta t\{F_{n-1}\} + \left(\alpha + \frac{1}{\vartheta}\Delta t\right)[M] r_{n-1} \\
&\quad + \left(\frac{1}{\vartheta}\right)[M]\frac{\partial r_{n-1}}{\partial t} + (\beta - (1-\vartheta)\Delta t)[K] r_{n-1}, \\
&\frac{\partial r_n}{\partial t} = \left(\frac{1}{\vartheta}\Delta t\right)(r_n - r_{n-1}) - \left(\frac{(1-\vartheta)}{\vartheta}\right)\frac{\partial r_n}{\partial t}, \\
&\frac{\partial^2 r_n}{\partial t^2} = \left(\frac{1}{\vartheta}\Delta t\right)\left(\frac{\partial r_n}{\partial t} - \frac{\partial r_{n-1}}{\partial t}\right) - \left(\frac{(1-\vartheta)}{\vartheta}\right)\frac{\partial^2 r_{n-1}}{\partial t^2},
\end{aligned} \tag{5}$$

where α and β: Rayleigh damping constant, Δt: time interval, t: time, F_n: load, r_n: displacement, n: time step, $[M]$: mass matrix, and $\vartheta = 0.5$ for Newmark-β method. When we subtract the elastic displacement by elastic calculation using G_0 from the elastic-plastic displacement by equivalent linearization technique, a plastic displacement is obtained.

3.3. Determination of Physical Parameters. The common parameters used in the static and dynamic analyses are wet density of soil ρ_t, elastic modulus E, and Poisson's ratio ν. Because the two analyses use the same elastic modulus E, the plastic displacement by dynamic response analysis is comparatively analogous to the displacement at collapse by static stability analysis. $\rho_t = 1.7$ g/cm^3, which is obtained by a density test. ν is assumed as 0.3. The horizontal displacement shown in Figure 4 is thought to be the combination of elastic and plastic displacements. Then, "average elastic displacement amplitude" is obtained by averaging the recoverable elastic displacement amplitudes in all vibration cycles. E is calculated as $G \times (1 + 2\nu)$. Damping constant h is assumed to be 0.3, because h affects little the dynamic response analysis in this case. Initial shear modulus G_0 in Hardin-Drnevich model is back-calculated from the average elastic displacement amplitude measured in test, by elastic analysis. As shown in Figure 13, the back-calculated G_0 is remarkably affected by acceleration amplitude. To relate the dynamic response

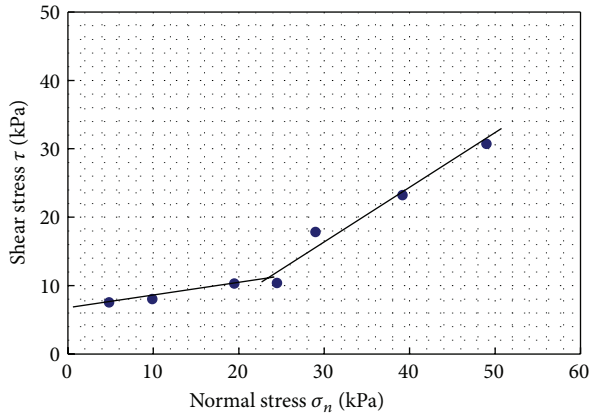

FIGURE 14: Strength parameters obtained from direct shear test with a constant pressure.

analysis to static stability analysis, G_0 is determined as the value at the intersection point of the curve A and curve B calculated using E, which is back-calculated by measured elastic displacement from a static model test. To simulate the actual state of model test, Mohr-Coulomb strength parameters c and φ are obtained by a direct shear test with a constant pressure of 29.4 kPa, as shown in Figure 14, in which a turning point is observed because the soil under the corresponding pressure before turning point is considered to be overconsolidated. Considering the compaction in entire manufacture process of vertical filling mentioned in Section 2.2, Mohr-Coulomb strength parameters in vibration model test are determined as $c = 6.87$ kPa and $\varphi = 10^\circ$ for overconsolidated state.

3.4. Comparisons between Test and Numerical Results. Based on the static stability analysis stated in Section 3.1, it is necessary to define the collapse state of slope for calculating the deformation at collapse. By stepwise increasing the horizontal seismic intensity k_h, the slope is gradually sliding into the collapse state, so the loading stage at which the yield elements are connected to form a global collapse mode first time is defined as the critical state. For ease of presentation, the definition is illustrated in Figure 15 by the evolution process of a slope collapse. As shown in Figure 15(a), the yield elements have not been connected at $k_h = 0.07$, while with the increase stepwise on k_h the yield region constructed by yield elements is gradually continuous when k_h reaches 0.10. By varying the horizontal seismic intensity k_h, the stability analysis is employed in search for the minimum k_h in which the yield elements are beginning to link up to create a collapse mode through the slope. From this, the slope failure is thought to occurr at $k_h = 0.10$, and accordingly the critical value of displacement for $k_h = 0.10$ can be calculated through static stability analysis.

According to the above definition, the slope failure occurs when $k_h = 0.27$ for the vertical slope without geotextile, and the corresponding elastic displacement is calculated by an elastic analysis. Subtracting the elastic displacement from the elastic-plastic displacement, we obtain the plastic displacement at collapse. Figure 16(a) shows the distribution of plastic displacement at collapse. Corresponding to the measured plastic displacement at collapse for point A in the range of 3.5~7.5 mm shown in Figure 6(a), the calculated plastic displacement at collapse is 4.78 mm. The distribution of yield elements is shown in Figure 17(a).

For the vertical slope with geotextile in the static stability analysis, the slope failure is defined at the seismic coefficient when the yield elements under the geotextile are connected. This is because the failure first occurs at the part around point B prior to the upper part. In our analysis, the failure occurs at $k_h = 0.5$. Figures 16(b) and 17(b), respectively, show the distributions of displacement at collapse and the corresponding yield regions. The calculated plastic displacement at collapse at point B (see Figure 1) is 1.4 mm that almost corresponds to the measured value shown in Figure 6(b). Compared with the nonreinforced case in Figure 3(a), the collapse mode in reinforced slope is restricted by earth reinforcement, which enlarges the elapsed time until collapse.

In the dynamic response analysis, Figures 18 and 19 compare the calculated average elastic displacement and the average plastic displacement with the test results. The results show that frequency produces an effect on the plastic displacements rather than the elastic results. The elapsed time until collapse T is calculated through (6). Figure 20 shows that the calculated elapsed time varies according to the acceleration amplitude and frequency, which shows a fairly accordance with the test shown in Figure 7. This means that the proposed procedure can evaluate the stability of slope to a considerable extent. One has

$$T = \frac{r_p}{(A_m \times f)}, \tag{6}$$

where $r_p = 4.78$ mm, plastic displacement at collapse; f: frequency; and A_m: amplitude of plastic displacement.

With respect to the vertical slope without geotextile, Figure 18(a) shows that the average elastic displacement increases with acceleration amplitude. Figure 19(a) shows the plastic displacements grow in proportion to the acceleration amplitude. Because the frequency of 7 Hz approximates the natural frequency of vertical slope, the average plastic displacement is greater than the 3 Hz, and T is shorter in 7 Hz than in 3 Hz as shown in Figure 20. It is also shown from Figures 7 and 20 that the elapsed time until collapse has shortened tendency as the acceleration amplitude increased.

For the vertical slope with geotextile, the calculated results are shown in Figures 18(b), 19(b), and 20. It is noticeable in three figures that the trends of variation of average elastic displacement, average plastic displacement and T with acceleration amplitude are consistent with the results without geotextile both in analysis and test. Note that there is no collapse in the reinforced slope for 200 gal of acceleration amplitude. As shown in Figure 20, both the analysis and test show that T for reinforced case is longer than that without geotextile due to the controls of geotextile on deformation of filling. Combining the equivalent linearization method in dynamic response analysis and the elastic plastic FEM in static stability analysis, the calculated average elastic displacement and the average plastic displacement as

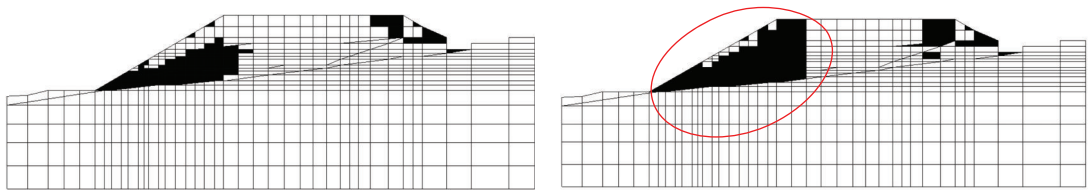

(a) $k_h = 0.07$ (b) $k_h = 0.10$

Figure 15: Definition of critical state.

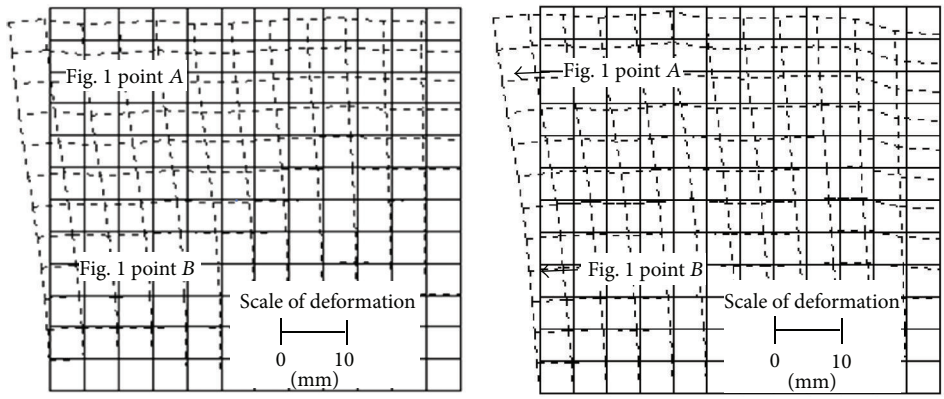

(a) Displacements of nonreinforced model slope (b) Displacements of reinforced model slope

Figure 16: Plastic displacement distribution at collapse.

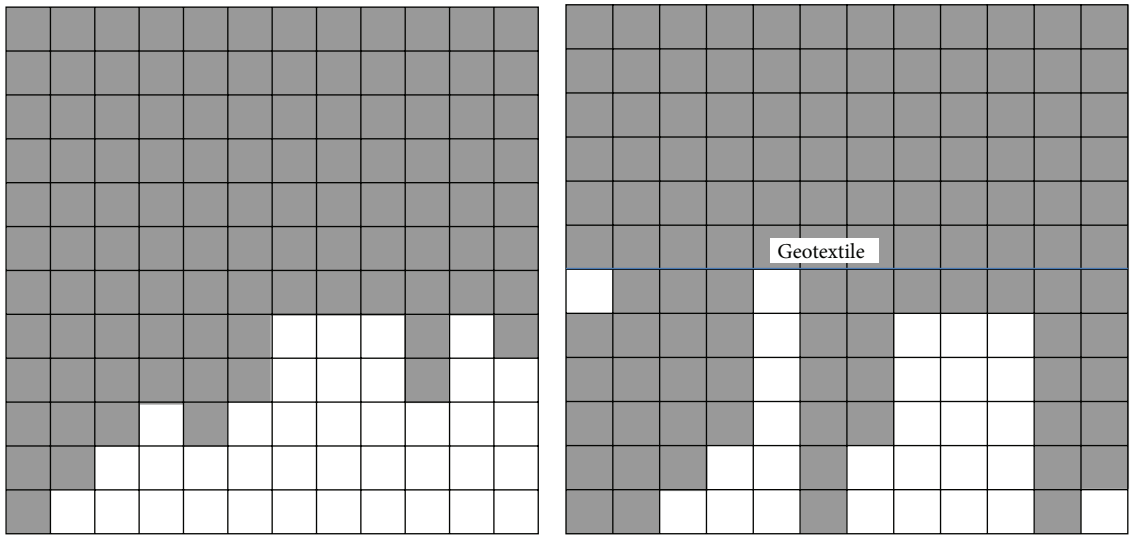

(a) Nonreinforced model slope (b) Reinforced model slope

Figure 17: Yield regions at collapse.

shown in Figures 18 and 19 agrees with the test results to some extent.

4. Results and Discussion

A lot of slope failures occurred on the Otaki village in the Nagano Ken-Seibu earthquake of magnitude 6.8, which occurred in the western part of Nagano prefecture on 1984 September, 14. From these actual cases, a large filling slope collapse at Mitsukoshi district in Otaki village is selected as the object of this research because the elapsed time from the commencement of earthquake to the collapse of the slope was detected. Figure 21 shows the geological full sections of collapsed slope [14], in which the geologic symbols are

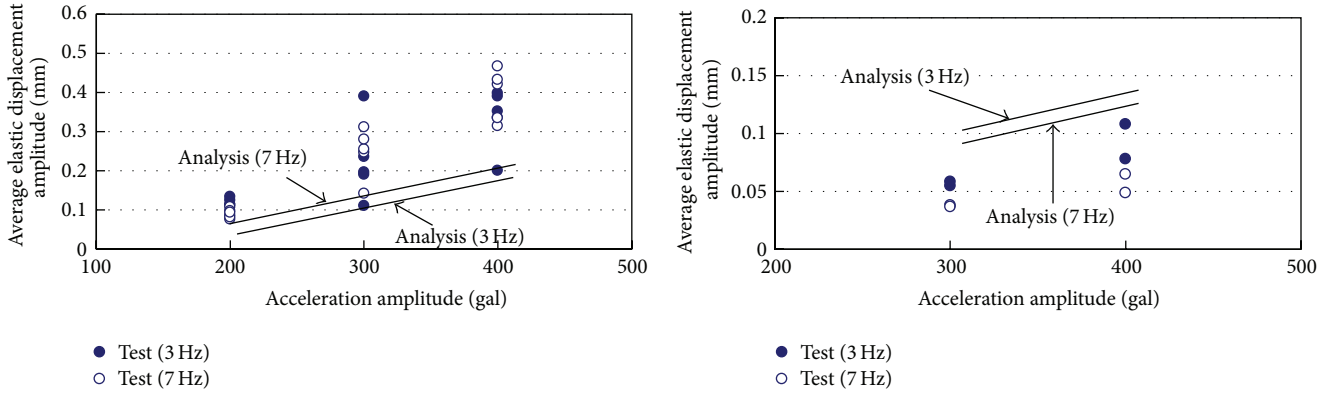

(a) Without geotextile (point A) (b) With geotextile (point B)

FIGURE 18: Comparison between calculated and measured average elastic displacements.

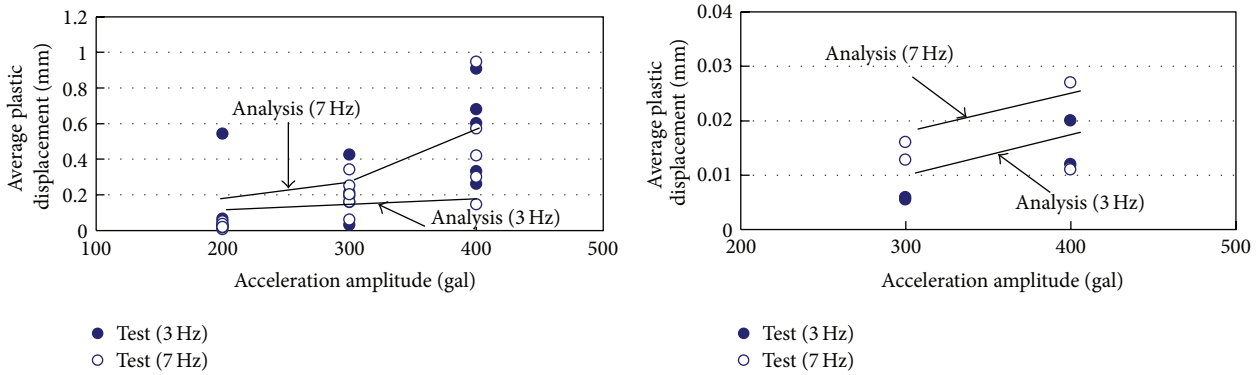

(a) Without geotextile (point A) (b) With geotextile (point B)

FIGURE 19: Comparison between calculated and measured average plastic displacements.

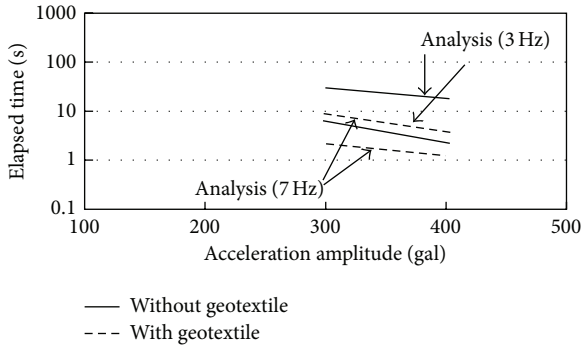

FIGURE 20: Comparison of time until collapse for reinforced and unreinforced cases.

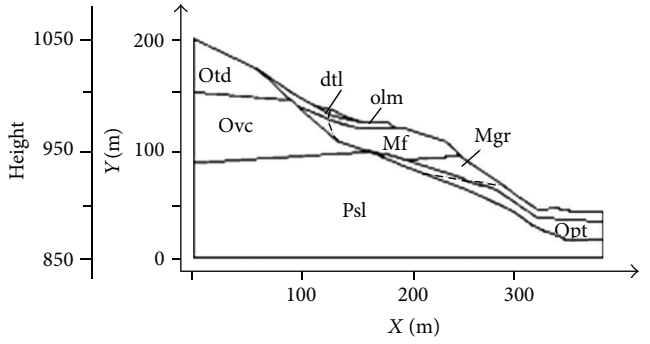

FIGURE 21: Geological full section of a slope collapse in the Nagano Ken-Seibu earthquake.

explained in Table 3. The slip surface represented by the broken line roughly occurred along the surface of Opt, which deposits on the bedrock. The maximum depth of fault plane is 35 m, and the fault length and width are 250 m and 150 m respectively, and the estimated the earthwork quantify of collapse is 2.7×10^5 m^3. Table 3 gives the stratum's parameters in geological formation shown in Figure 21, in which the curve number denotes the relationships between G/G_0 and h versus shear strain applied in analysis, as shown in Figure 22 and V_s is rate of shear wave of soil stratum.

The time history of response acceleration used in this study is provided as Figure 23 by Applied Geology Company, which is based on the strong motion seismograms recorded

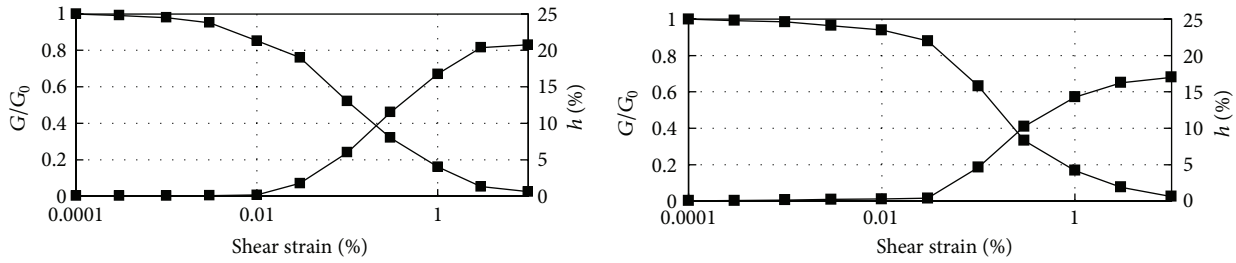

(a) Curve number ①

(b) Curve number ②

Figure 22: Relation curves between G/G_0 and h versus shear strain corresponding to Table 3.

Table 3: Stratum's parameters [14].

Sym.	Geologic formations	γ_t kN/m^3	V_s m/s	G_0 kN/m^3	h %	ν	Curve Number	c kPa	φ °
dtl	Talus deposit	17.4	140	34323	5	0.49	②	19.6	35
olm	Loam	13.6	160	35304	5	0.49	②	53.9	20
Mf	Mud flow deposit	18.3	230	99047	5	0.49	①	53.9	20
Mgr		18.9	280	151022	5	0.49	①	19.6	35
Opt	Pyroclastic tuff	14.5	210	58840	5	0.49	②	44.1	21
Otd	Tuff breccia	25.5	600	931632	5	0.3	—	98.1	45
Ovc	Volcanic puddingstone	25.5	620	980665	5	0.3	—	98.1	45
Psl	Slate	26.5	1250	4216860	2	0.3	—	147.1	45

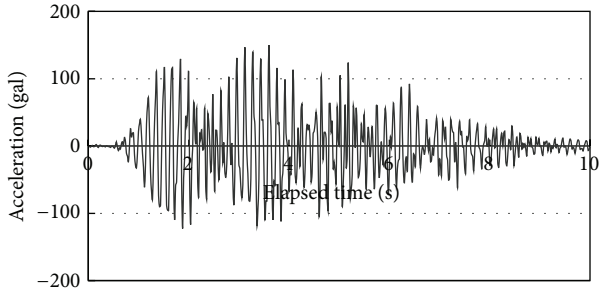

Figure 23: Time history of response acceleration.

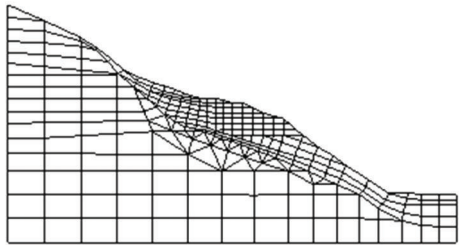

Figure 24: FE meshing of the case study.

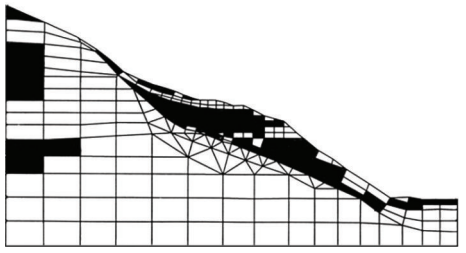

Figure 25: Collapse mode at $k_h = 0.12$.

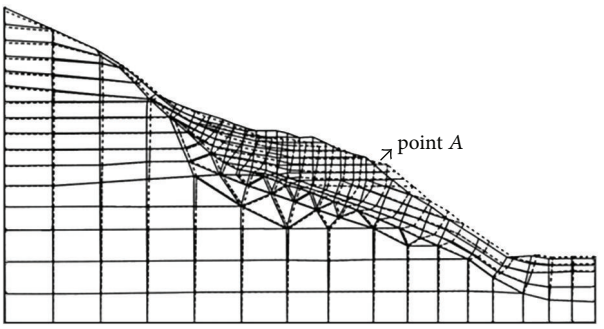

Figure 26: Distribution of plastic displacement at $k_h = 0.12$.

on the stations of Japan Meteorological Agency near to the epicenter [19].

The FE meshing for the actual filling slope is shown in Figure 24. In the static stability analysis, the collapse is considered to be the critical state forming a global collapse mode by connecting the yield elements from the surface of the slope to the slope end. Based on the above definition of collapse, the iterative procedure is performed by increasing

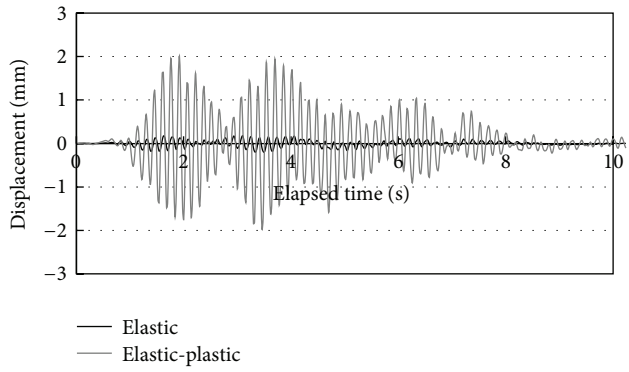

Figure 27: Elastic and elastic-plastic displacements.

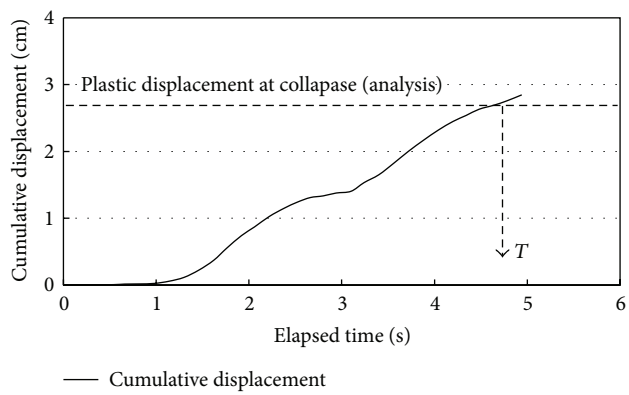

Figure 28: Cumulative plastic displacement.

the horizontal seismic intensity k_h and the yield elements create a continuous yield region when $k_h = 0.12$, as shown in Figure 25. Correspondingly, the distribution of plastic displacement is shown in Figure 26, in which the horizontal plastic displacement of point A just before slope reaches its maximum. According to the static analysis, the calculated plastic displacement at collapse of point A is 2.7 cm. In the dynamic response analysis, the time interval is 0.02 s. Because the input acceleration shown in Figure 22 is irregular wave, it is impossible to demand an average plastic displacement as described previously for sin waves. For this actual case, the plastic displacement of each seismic wave is calculated by subtracting the elastic component from the elastic plastic amplitude for the current wave, as shown in Figure 27. The calculated cumulative plastic displacement for each of the actual seismic wave in dynamic response analysis is shown in Figure 28. When the cumulative displacement reaches 2.7 cm of plastic displacement at collapse obtained from the static analysis, the value of T corresponds to 4.78 seconds in Figure 28, which is approximate with the observed collapse time of 5 seconds.

5. Conclusions

The shaking table tests of vertical slope showed that the plastic displacement just before collapse is constant regardless of acceleration amplitude and frequency. This result indicates a new aspect of slope stability, that a slope failure during earthquake occurs when a cumulative plastic displacement of slope exceeds a critical value of plastic displacement. Based on this aspect, this paper proposed a numerical procedure, in which the cumulative plastic displacement is calculated by a dynamic response analysis using an actual seismic wave, in which the critical value of plastic displacement is estimated by a static stability analysis considering seismic coefficient.

The proposed procedure was applied to the laboratory model tests to examine the numerical characteristics and applicability of the proposed procedure. Comparison between the unreinforced and reinforced slopes showed that the earth reinforcement can constrain the deformation of slope and extend the elapsed time until collapse to enhance stability of slope because it restricts the development of collapse through slope. The calculated displacement and the elapsed time until collapse T are fairly close to the test results and showed the same tendency of variation with the acceleration amplitude a_m and frequency f. This means that the proposed procedure is applicable to evaluate the stability of slope to a considerable extent.

The proposed procedure was applied to an actual filling slope failure during earthquake with an exact collapse time provided by witness. Combining the dynamic response analysis with the static stability analysis, the proposed procedure calculated an approximate elapsed time until collapse T with observed time. The application of the proposed procedure to the laboratory model tests and case study shows the possibility that the proposed procedure gives realistic predictions and provides a useful engineering tool to evaluate the slope stability during earthquake.

Conflict of Interests

The authors declare that there is no conflict of interests regarding the publication of this paper.

Acknowledgments

This work has been supported by the National Science Foundation of China (no. 51409025), the Chongqing Natural Science Foundation (no. cstc2012jjA0510), the Fundamental Research Funds for the Central Universities (no. CDJZR12200011), and the State Education Ministry and the CQJTU Scientific Research Foundation (no. 2013kjc009).

References

[1] D. Eberhart-Phillips, P. J. Haeussler, J. T. Freymueller et al., "The 2002 Denali fault earthquake, Alaska: a large magnitude, slip-partitioned event," *Science*, vol. 300, no. 5622, pp. 1113–1118, 2003.

[2] P. Cui, X.-Q. Chen, Y.-Y. Zhu et al., "The Wenchuan Earthquake (May 12, 2008), Sichuan Province, China, and resulting geohazards," *Natural Hazards*, vol. 56, no. 1, pp. 19–36, 2011.

[3] L. Zhang, J. H. Liu, H. Y. Fu, and Z. Guo, "Analysis on dynamic stability of rock slope in seismic area in Sichuan Province," in *Advances in Unsaturated Soil, Geo-Hazard, and*

Geo-Environmental Engineering, vol. 217, pp. 188–194, Geotechnical Special Publication, 2011.

[4] N. Ambraseys and M. Srbulov, "Earthquake induced displacements of slopes," *Soil Dynamics and Earthquake Engineering*, vol. 14, no. 1, pp. 59–71, 1995.

[5] JSCE, *Energy Facilities, Dynamic Analysis and Earthquake Resistant Design*, Gihodo Press, 1989, (Japanese).

[6] S. K. Sarma, "Seismic stability of earth dams and embankments," *Geotechnique*, vol. 25, no. 4, pp. 743–761, 1975.

[7] R. W. Jibson, "Methods for assessing the stability of slopes during earthquakes—a retrospective," *Engineering Geology*, vol. 122, no. 1-2, pp. 43–50, 2011.

[8] J. D. Bray and T. Travasarou, "Pseudostatic coefficient for use in simplified seismic slope stability evaluation," *Journal of Geotechnical and Geoenvironmental Engineering*, vol. 135, no. 9, pp. 1336–1340, 2009.

[9] M. Matsuo, K. Itabashi, and Y. Sasaki, "Study on aseismicity of earth structures by inverse analyses of actual cases," *Proceedings of the Japan Society of Civil Engineers*, vol. 343, pp. 25–33, 1984.

[10] S. Ohtsuka and M. Matsuo, "Rigid plastic dynamic deformation analysis of soil structures," in *Proceedings of the 1st International Conference on Earthquake, Geotechnical Engineering*, vol. 2, pp. 1147–1152, Tokyo, Japan, 1995.

[11] J. D. Bray, A. J. Augello, G. A. Leonards, P. C. Repetto, and R. J. Byrne, "Seismic stability procedures for solid-waste landfills," *Journal of Geotechnical Engineering*, vol. 121, no. 2, pp. 139–151, 1995.

[12] S. L. Kramer and M. W. Smith, "Modified Newmark model for seismic displacements of compliant slopes," *Journal of Geotechnical Engineering*, vol. 123, no. 7, pp. 635–644, 1997.

[13] J. D. Bray and E. M. Rathje, "Earthquake-induced displacements of solid-waste landfills," *Journal of Geotechnical and Geoenvironmental Engineering*, vol. 124, no. 3, pp. 242–253, 1998.

[14] Japanese Geotechnical Society, *Research Council Report on Mechanism and Design of Stability of Slope in Earthquake*, 1999, (Japanese).

[15] O. C. Zienkiewicz, S. Valliappan, and I. P. King, "Stress analysis of rock as a 'no tension' material," *Geotechnique*, vol. 18, no. 1, pp. 56–66, 1968.

[16] O. C. Zienkiewicz, S. Valliappan, and I. P. King, "Elasto-plastic solutions of engineering problems "initial stress" finite element approach," *International Journal for Numerical Methods in Engineering*, vol. 1, pp. 75–100, 1969.

[17] G. C. Nayak and O. C. Zienkiewicz, "Elasto-plastic stress analysis. A generalization for various constitutive relations including strain softening," *International Journal for Numerical Methods in Engineering*, vol. 5, no. 1, pp. 113–135, 1972.

[18] I. M. Smith, *Programming the Finite Element Method with Application to Geomechanics Manchester*, John Wiley & Sons, 1982.

[19] S. Yoshida and K. Koketsu, "Simultaneous inversion of waveform and geodetic data for the rupture process of the 1984 Naganoken-Seibu, Japan, earthquake," *Geophysical Journal International*, vol. 103, no. 2, pp. 355–362, 1990.